Energy Conversion and Management: X 21 (2024) 100509

Contents lists available at ScienceDirect

Energy Conversion and Management: X

journal homepage: www.sciencedirect.com/journal/energy-conversion-and-management-x

Enhancing efficient solar energy harvesting: A process-in-loop investigation of MPPT control with a novel stochastic algorithm

Muhammad Kamran Khan [a], Muhammad Hamza Zafar [b], Talha Riaz [c], Majad Mansoor [d], Naureen Akhtar [b,*]

[a] School of Technology and Innovations, University of Vaasa, Finland
[b] Department of Engineering Sciences, University of Agder, NO-4879 Grimstad, Norway
[c] Faculty of Engineering Sciences and Technology, Hamdard University, Islamabad
[d] Ningbo China Institute for Supply Chain Innovation Ningbo, 315000, China

ARTICLE INFO

Keywords:
Partial shading (PS)
Photovoltaic (PV)
Energy valley optimizer (EVO)
Particle swarm optimization (PSO)
Complex partial shading (CPS)
Maximum power point tracking (MPPT) controller

ABSTRACT

PV systems currently generate 4% of the world's energy needs, and their share is growing quickly. The maximum power point tracking (MPPT) is a complex non-convex optimization problem because the electrical characteristics of the PV model are nonlinear. Changes in temperature, partial shading (PS), and irradiance levels can all affect the amount of power that can be extracted from the solar system. Therefore, in this work, a novel energy valley optimizer (EVO) based MPPT algorithm is suggested to extract maximum power from solar. The classical perturb and observe (P&O), whale optimizer algorithm (WOA), cuckoo search algorithm (CSA), and particle swarm optimization (PSO) algorithms are all compared to EVO. Five case studies, including a field atmospheric data study, partial shading, variable temperature, and irradiance, are used to conduct in-depth analytical and statistical analysis. Furthermore, the successful verification of the MPPT control algorithm on the real microcontroller (Arduino MKRZERO board) through the PIL test is a critical milestone in this research. Quantitative, comparative, statistical and experimental results indicate that the proposed EVO-based MPPT achieves superior performance through 30% quicker tracking time and 80% faster settling time, which result in 4–8% higher power efficiency. The results indicate that the suggested MPPT controller successfully addresses the shortcomings of the current MPPT methods.

1. Introduction

The most affordable and thoroughly researched source of renewable energy is solar power. PV modules transform solar energy into the most efficient form of electricity. The rapid expansion of PV systems is primarily due to improvements in manufacturing processes, material science, and supportive legislation. The primary characteristics for PV systems are the low carbon emission, scalability and simplicity of installation [1,2]. Solar energy from PV systems is converted into electrical energy, the most controllable type of energy in the utility grid.

Improvements are always being made to improve PV system performance. Maximum power point tracking (MPPT) is the main issue with PV system control. The MPPT is a difficult optimization control problem because the electrical characteristics of the PV model are nonlinear [3]. Second, operating factors like temperature (T) and irradiance (G) might affect the operating point [4]. The uneven irradiance distribution across the series–parallel coupled PV panels is the third issue [5,6].

Partial shading (PS), is a fundamental reason why traditional MPPT approaches fail to track maximum power. The primary requirements for PV systems are quick MPP tracking, high efficiency, and minimal oscillations in voltage transients. Inverters and DC converters are used to interface power generation and load [7]. By precisely adjusting the duty cycle, the PV system can be run on MPP. The GMPP can be shifted by the changes in irradiance and temperature. As a result, it's important to actively monitor the MPP. Fig. 1 shows a typical PV setup (see Fig. 2 and Fig. 3).

In literature, numerous standard and unconventional modern intelligence techniques have been researched [8,9]. These techniques are broken down into numerous categories based on elements including the tracking method, controllers, hardware, and ease of execution. The gradient based conventional techniques include adopted perturb and observe (P&O) [10], hill climbing (HC) [11], and incremental

* Corresponding author.
E-mail address: naureen.akhtar@uia.no (N. Akhtar).

https://doi.org/10.1016/j.ecmx.2023.100509
Received 16 August 2023; Received in revised form 3 December 2023; Accepted 5 December 2023
Available online 7 December 2023

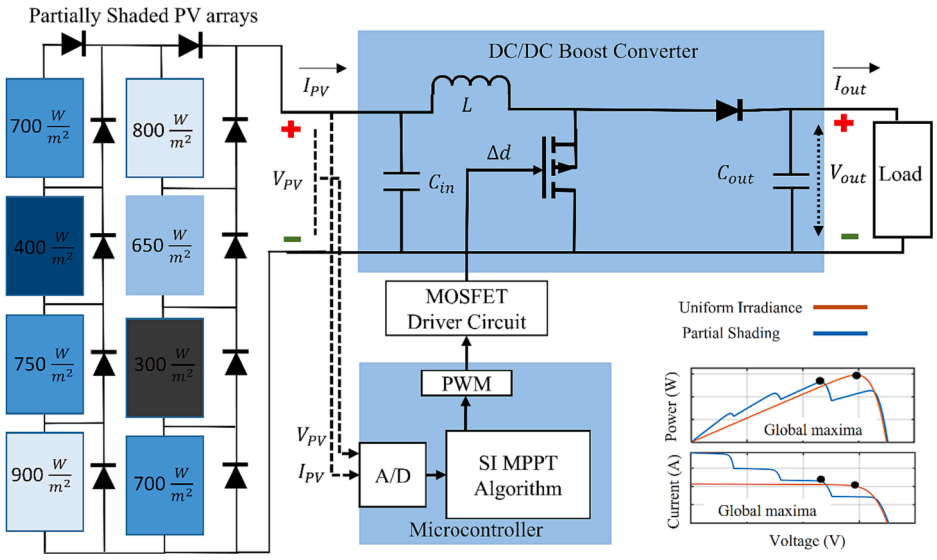

Fig. 1. Block diagram of MPPT controller under partial shading conditions.

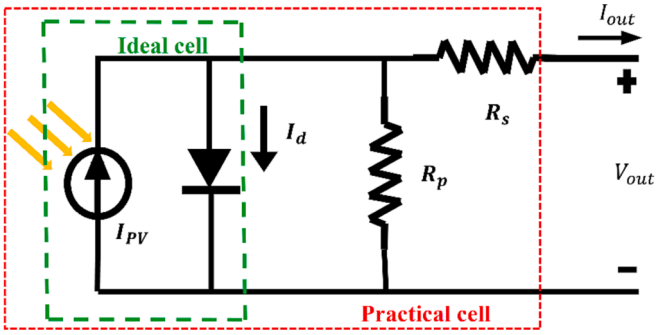

Fig. 2. A single diode model of PV cell.

conductance (IC) [12]. Despite being easy to use, these approaches cause undesirable oscillations around GM. Due to a single solution failing to detect the PS, there is a significant power loss. As a result, efficiency is severely diminished. Due to their inability to distinguish between several maxima, classical approaches lose a significant amount of power [13]. Alternatively, artificial intelligence techniques have recently been researched for MPPT [14,15]. High computational resource requirements, algorithm complexity, storage burden and pricey microcontrollers are major downsides of these soft computing techniques.

In the past decade a variety of stochastic algorithms have been used for the MPPT of PV systems [16,17]. The primary benefit of evolutionary algorithms over competing technologies is their ability to track GM under PS conditions. Search and rescue algorithm (SRA) [18],particle swarm optimization (PSO), most valuable player algorithm (MVPA), earthquake optimization algorithm [19], grey wolf optimizer (GWO) [20],grass hopper optimization (GHO) [21], musical chairs algorithm (MCA) [22] and atomic orbital search (AOS) [23] are some of the examples of metaheuristic based MPPT algorithms. The parameters that impact how well these algorithms' function include population size, exploration capabilities, iterations, exploitation capabilities and parametric adjustment. These strategies search for the optimal position using randomly initialized populations and particles. These MPPT-based optimization strategies perform significantly differently depending on the parameter adjustments and starting population distribution.

In order to fine-tune the controller settings under uniform and partial shade situations, a combinatorial MPPT algorithm based on the fuzzy logic controller (FLC) and improved farmland fertility optimization (IFFO) approach was proposed in [24]. The authors claimed an efficiency of 99 %. In order to reduce the oscillations around GMPP, a novel metaheuristic technique called the opposition-based equilibrium optimizer (OBEO) algorithm was employed in [25]. The proposed technique has an efficiency of 95.09 % under dynamic PSC, 96.17 % under uniform PSC, and 86.25 % under complicated PSC. Two hybrid *meta*-heuristic methods were used in [26] to enhance the MPPT of solar systems. The Whale Optimization Algorithm and the Differential Evolution algorithms serve as the foundation for the first proposed maximum power point tracking method. Both methods were quite effective at increasing

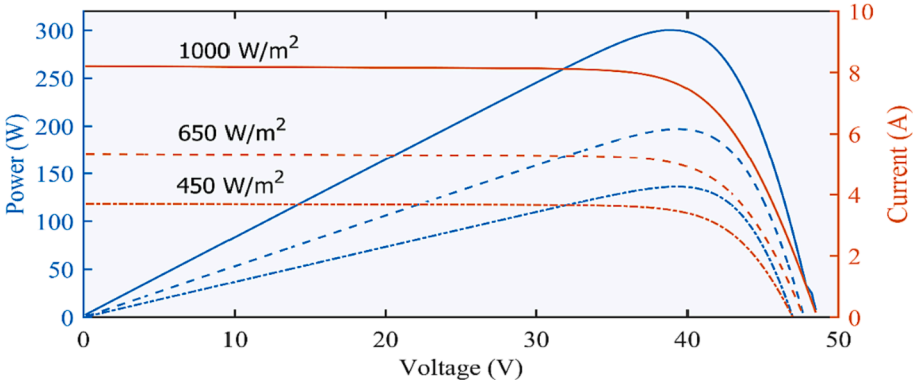

Fig. 3. The PV system P-V & VI characteristics.

the solar system's effectiveness in both uniform and shaded conditions. A new hybrid MPPT method built on the Genetic Algorithm (GA) and fractional open circuit voltage (FOCV) was suggested in [27]. The proposed technique only relies on one decision variable resulting in reduced complexity and convergence time. The results showed that the suggested methodology outperformed the traditional FOCV method by about 3 % with very little steady-state oscillations.

1.1. Motivation & contribution

In this research, a new dynamic study is developed and put into practice to lessen the restriction of slow tracking time of conventional MPPT approaches. In this work, a novel metaheuristic algorithm, called Energy valley optimizer (EVO), is suggested to track the global maxima. To efficiently track GMPP under a variety of challenging PS situations, the starting particles in the EVO MPPT technique are spread throughout the possible feasible space by traversal search in the global mode. The primary benefits and novel features of the suggested method are:

In comparison to the MPPT techniques found in the literature, proposed method tracks the global maxima in every iteration of the reference voltage.
In the EVO MPPT technique, the necessary duty cycle of the converter is estimated based on the mathematical model of the natural phenomenon of the electron stability. The mathematical model ensures the maximum power of PV system under every irradiance pattern.
Proposed technique has low implementation complexity and low calculation workload, which result in the use of cheaper controller.
Verification of the proposed MPPT control algorithm on the real microcontroller (Arduino MKRZERO board) through the PIL test.

The remainder of the work is broken up into five sections. The statement of the problem and the PV system modelling are presented in Section 2. EVO based MPPT is introduced in the second section 3. The results and experimental verifications are presented in section 4. Section 5 discuss the results and section 6 presents the conclusion.

2. PV system modelling

2.1. PV model under STC and PS conditions

Many equivalent designs have been presented to analyze how PV module interact with the environment. To lessen the effects of external variations like temperature and irradiance, model should have a DC current source and an antiparallel diode. The behavior of diode current (I_d) is provided by equation (2). Eq. (2), however, falls short of accurately describing PV behavior. Practically, intrinsic resistance additions are included to accurately describe the PV behavior in Eq. (3).

$$I_{out} = I_{PV} - I_d \tag{1}$$

$$I_{out} = I_{PV} - I_0\left[\exp\left(\frac{V_{out}}{\hat{I} \pm V_T}\right) - 1\right] \tag{2}$$

$$I_{out} = I_{PV} - I_0\left[\exp\left(\frac{V_{out} + I_{out}R_s}{\hat{I} \pm V_T}\right) - 1\right] - \left(\frac{V_{out} + I_{out}R_s}{R_p}\right) \tag{3}$$

$$V_T = \frac{N_s kT}{q} \tag{4}$$

Eq. (5) specifies how to combine PV cells in series and parallel to scale up the output capacity of a PV system.

$$I_{out} = I_{PV}N_p - N_pI_0\left[\exp\left(\frac{V_{out} + I_{out}R_{s\,eq}}{N_s\hat{I} \pm V_T}\right) - 1\right] - \left(\frac{V_{out} + I_{out}R_{s\,eq}}{R_{p\,eq}}\right) \tag{5}$$

Table 1
PV cell and arrays Electrical parameters.

Symbol	Description
V_{out}	Output voltage
N_s	Series connected cells
I_{PV}	Cell current
B	Boltzmann constant $=1.38073 \times 10-23J/K$
I_{PV-STC}	Cell current at STC conditions
V_T	Thermal voltage
R_s	Equivalent resistance in series
R_{peq}	Total Equivalent parallel resistance array
I_o	Reverse saturation current
I_d	Diode current
R_{seq}	Equivalent series resistance array
N_p	Parallel connected cells
R_p	parallel resistance
K_I	Short circuit current constant
G	Irradiance (W/m^2)
a	Diode ideality factor
T	Temperature (°C)
T_{STC}	Temperature at STC condition (25°C)
G_{STC}	Irradiance at STC condition ($1000W/m^2$)

Table 2
Kyocera KD320GX-LFB > 320 W solar panel electrical characteristics.

Electrical Characteristics	Kyocera KD-320GX LFB > 320 W
Maximum power (P_{max}) at STC	320 W
MPP voltage (V_{mpp})	40.1 V
MPP current (I_{mpp})	7.99 A
V_{oc}	49.5 V
I_{sc}	8.60 A
Diode ideality factor	0.99412

As seen in Eq. (6), the current generated by PV cells is strongly influenced by two key variables: operating temperature (T) and irradiance level (G).

$$I_{PV} = (I_{PV\text{-}STC} + B_I(T - T_{STC}))\cdot G/G_{STC} \tag{6}$$

According to Eq. (6), there is a direct relationship between output current and irradiance. The description of parameters, variables and constants is given in Table 1.

Photovoltaic system is a combination of PV arrays. The electrical characteristics of cell, arrays and system are the same. The electrical characteristics for the Kyocera KD320GX-LFB PV arrays are presented in Table 2.

2.2. Partially shaded arrays and effects of bypass diode

PV arrays receiving varying amounts of irradiance produce mismatched currents when connected in series. Bypass diodes have the ability to sustain higher current in PS modules, as demonstrated in Fig. 4. As a result, the nonlinear MPPT problem transforms into a multiple-LM non-convex optimization problem [28]. Fig. 5 (a) and (b) show bypass diode effect on P-V and I-V curves under four PS patterns, respectively. The GMs range in voltage from 80 to 180 V.

2.3. Boost converter

Boost converter provides the load interfacing and control action. The components value and parameters are calculated using Eq. (7)-(11). The MPPT control regulates the voltage V_{pvh} of PV system to adapt the best V_{refh} at GM which is further explained in tracking mechanism. The duty cycle ($d_{cycle}[0, 1]$) is modulated to adjust V_{pv} at V_{refh}.

$$v_{dcout} = \frac{v_{dcin}}{1 - d_{cycle}} \tag{7}$$

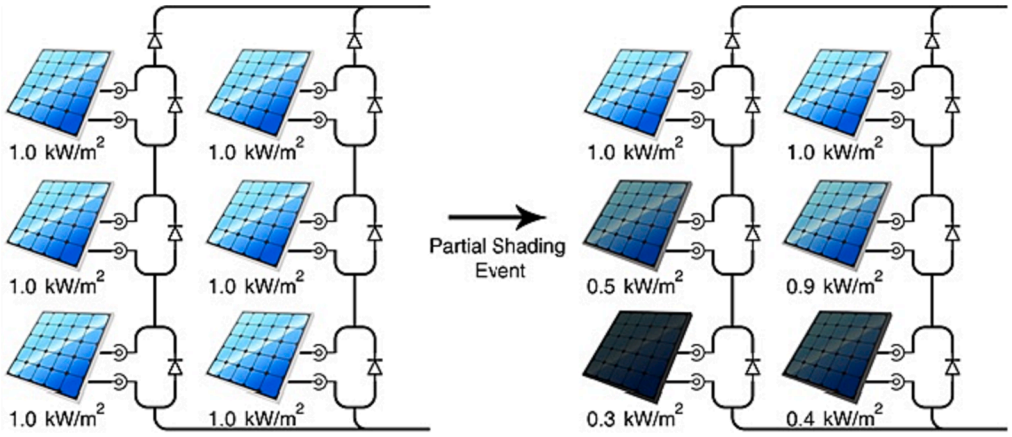

Fig. 4. The partial shading event with blocking and bypass diodes.

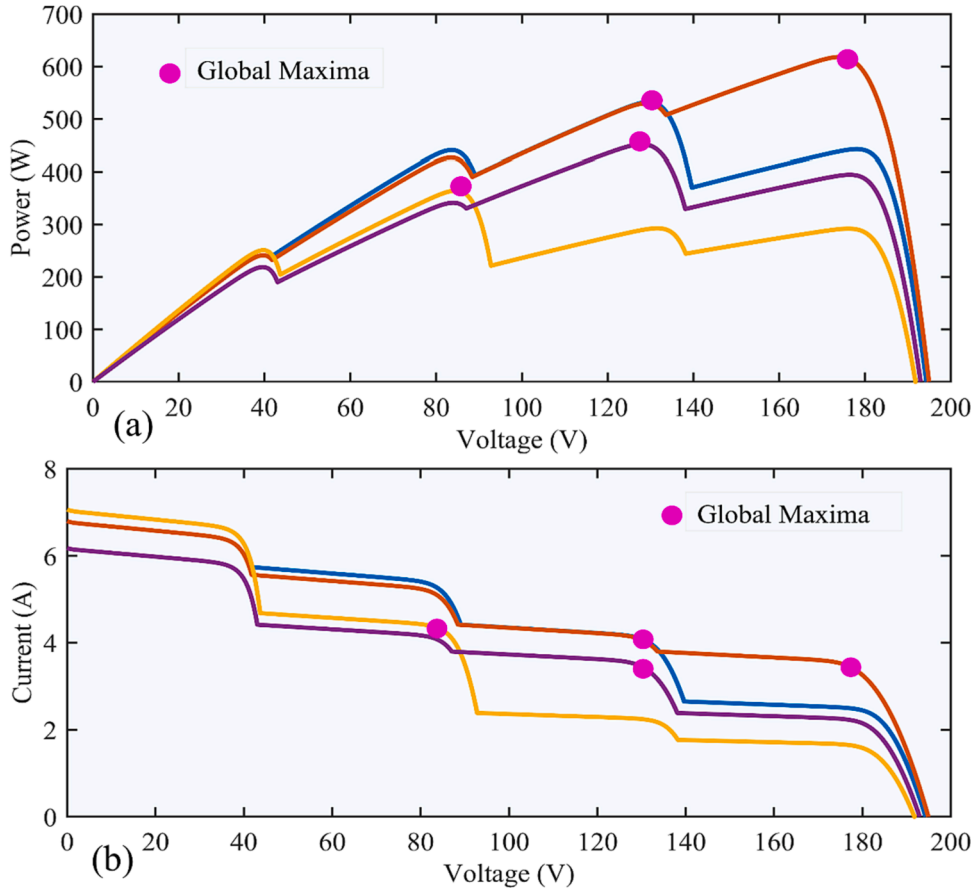

Fig. 5. (a) The P-V behavior under PS condition (b) The I-V behavior under PS conditions.

$$d_{cycle} = \frac{t_{on}}{t_{swt}} \tag{8}$$

$$c_{i\lambda} = \frac{\Omega i_{id}}{8\Omega i_{id} f_{swt}} \tag{9}$$

$$L = \frac{V_{pvh} d_{cycle}}{2\Omega i_{id} f_{swt}} \tag{10}$$

$$c_{o\lambda} = \frac{i_o d_{cycle}}{8\Omega v_{id} f_{swt}} \tag{11}$$

The input–output capacitances are denoted by $C_{i\lambda}$, and $C_{o\lambda}$ respectively. The Ωv_{ld} represent ripple voltage, Ωi_{ld} is inductor ripple current and v_{dcout} represents the converter output voltage.

2.4. Partial shading condition

When PV modules in a PV system cannot get equal irradiation, the PS happens [29]. The number of Partial shaded modules is equal to the number LM peaks. Classical convex optimization techniques usually failed to distinguish between several local Maximas formed due to partial shading, resulting in a loss of significant amount of solar power.

3. Proposed methodology

3.1. Energy valley optimizer

The Energy Valley Optimizer (EVO) is a revolutionary metaheuristic algorithm that is inspired by the physical phenomenon of particle stability and decay modes [30]. One of the most prominent characteristics of a chemically unstable element is its decay rate which is a process in which low energy particles are generated. One parameter to consider is the N/Z ratio in which N represents the number of neutrons while Z represents the number of protons. Each particle tries to improve its stability by changing N/Z ratio. Basically, three particles are emitted namely alpha particles, beta particles and gamma particles. Emission of alpha particles results in a decrease in the N/Z ratio while emission of beta particle N/Z ratio while N/Z ratio remain unchanged during gamma decay. The tendency of a particle to reach a stable point after decay can be used to improve the solution of the metaheuristic algorithm.

3.1.1. Mathematical model

In the first step, different solution candidates in the proposed solution are considered as particles with different stability levels.

$$X=\begin{bmatrix}X_1\\X_2\\.\\.\\X_i\\.\\.\\X_n\end{bmatrix}=\begin{bmatrix}x_1^1x_1^2\ldots x_1^j\ldots..x_1^d\\x_2^1x_2^2\ldots x_2^j\ldots..x_2^d\\.\\.\\x_i^1x_i^2\ldots x_i^j\ldots..x_i^d\\.\\.\\x_n^1x_n^2\ldots x_n^j\ldots..x_n^d\end{bmatrix},\begin{cases}i=1,2,3,\ldots.n\\j=1,2,3,\ldots.d\end{cases} \tag{12}$$

$$x_i^j=x_{i,min}^j+rand.\left(x_{i,max}^j-x_{i,min}^j\right),\begin{cases}i=1,2,3,\ldots.n\\j=1,2,3,\ldots.d\end{cases} \tag{13}$$

where, n represents the total number of particles i.e.; solutions available, d is the dimensions of the problem under consideration, x_i^j the decision variable at the j th position of an i th candidate, $x_{i,min}^j$ and $x_{i,max}^j$ show lower and upper bounds respectively. The *rand* is a randomly generated variable in the range of [0,1]. In the next step, the boundary is defined based on neutron enrichment level. This parameter is known as Enrichment Bound (EB) which considers Neutron Enrichment Level (NEL) and is mathematically defined as follows:

$$EB=\frac{\sum_{i=1}^{n}NEL_i}{n},i=1,2,3,\ldots.n \tag{14}$$

The stability levels of various solutions are established in the third phase while taking into account the assessments of the objective function:

$$SL_i=\frac{NEL_i-BS}{WS-BS},i=1,2,3,\ldots.n \tag{15}$$

The best minimum and worst maximum values for objective function values are BS and WS, respectively, where SL_i is taken to represent the stability level.

If the stability level of a particle has greater value as compared to the stability bound, then alpha and gamma decay is considered as they are suitable for a heavier particle with comparatively higher stability level. Therefore, emission of alpha rays can be considered in order to improve the particle's stability which can be represented mathematically as follows:

$$X_i^{New1}=X_i(X_{BS}(x_i^j)),\begin{cases}i=1,2,3,\ldots.n\\j=Alpha\ index\ II\end{cases} \tag{16}$$

The EVO positions are updated using the above formula, and a new candidate is created. Two random integers are created for this purpose; one is *AlphaindexI* in the range of [1, d] and indicates the number of rays to be released, while the other is *AlphaindexII* in the range of [1, *AlphaindexI*] specifies the release of particular alpha rays.

Similarly, emission of gamma rays also results in the stability of the particle and can be considered as another position updating system which generates a new solution. For this reason, two different random integers are generated namely *GammaindexI* which ranges between [1, d] denoting the number of emitted photons and *GammaindexII* which ranges between [1, *GammaindexI*]. The distance between the particle under consideration and other particles is calculated using the following mathematical relationship:

$$D_i^k=\sqrt{(x_2-x_1)^2+(y_2-y_1)^2},\begin{cases}i=1,2,3,\ldots.n\\k=1,2,3,\ldots.n-1\end{cases} \tag{17}$$

Here, D_i^k is the total distance between the i th particle and its k th neighboring particle while (x_1,y_1) and (x_2,y_2) represents the coordinates of the particle available in the search space. The second solution candidate is calculated as follows:

$$X_i^{New2}=X_i(X_{NG}(x_i^j)),\begin{cases}i=1,2,3,\ldots.n\\j=Gamma\ index\ II\end{cases} \tag{18}$$

Where X_i^{New2} = newly generated particle in the solution space, X_i is the current position vector of the i th particle, x_i^j is the decision variable and X_{NG} represent the position vector of the neighboring particle.

When a particle's stability level is below the stability bound, beta decay is taken into account. In beta decay, a method is used to update the particle's position by moving it in the direction of the candidate with the best stability (X_{BS}) and the particle's center (X_{CP}). These characteristics of the algorithm helps in imitating the particles tendency to reach to stability.

$$X_{CP}=\frac{\sum_{i=1}^{n}X_i}{n},i=1,2,3,\ldots.n \tag{19}$$

$$X_i^{New1}=X_i+\frac{(r_1\times X_{BS}-r_2\times X_{CP})}{SL_i},i=1,2,3,\ldots.n \tag{20}$$

Where X_i^{New1} and X_i are the upcoming and the current position vectors for the i th particle, X_{CP} is the position vector for the center of particles.

To improve the performance of the algorithm, another system is introduced which results in the movement of the particle towards the particle with the best stability and neighboring particle and this movement is not affected by particle's stability level. It is formulated mathematically as follows:

$$X_i^{New2}=X_i+(r_3\times X_{BS}-r_4\times X_{NG}),i=1,2,3,\ldots.n \tag{21}$$

Where X_i^{New2} and X_i are the updated and current position while r_3 and r_4 are random variables determining the amount of particles movement.

For a particle with neutron enrichment level lower than the enrichment bound, the particles tend to either emit positrons or capture electrons. The movement of the particle can be represented as follows:

$$X_i^{New}=X_i+r,i=1,2,3,\ldots.n \tag{22}$$

Where X_i^{New} and X_i are the new and the current position of the i th particle and r is the random variable between 0 and 1.

3.1.2. Stopping criterion

The two-stopping criterion are taken into account in this investigation. The first is the maximum number of iterations. In this study, the

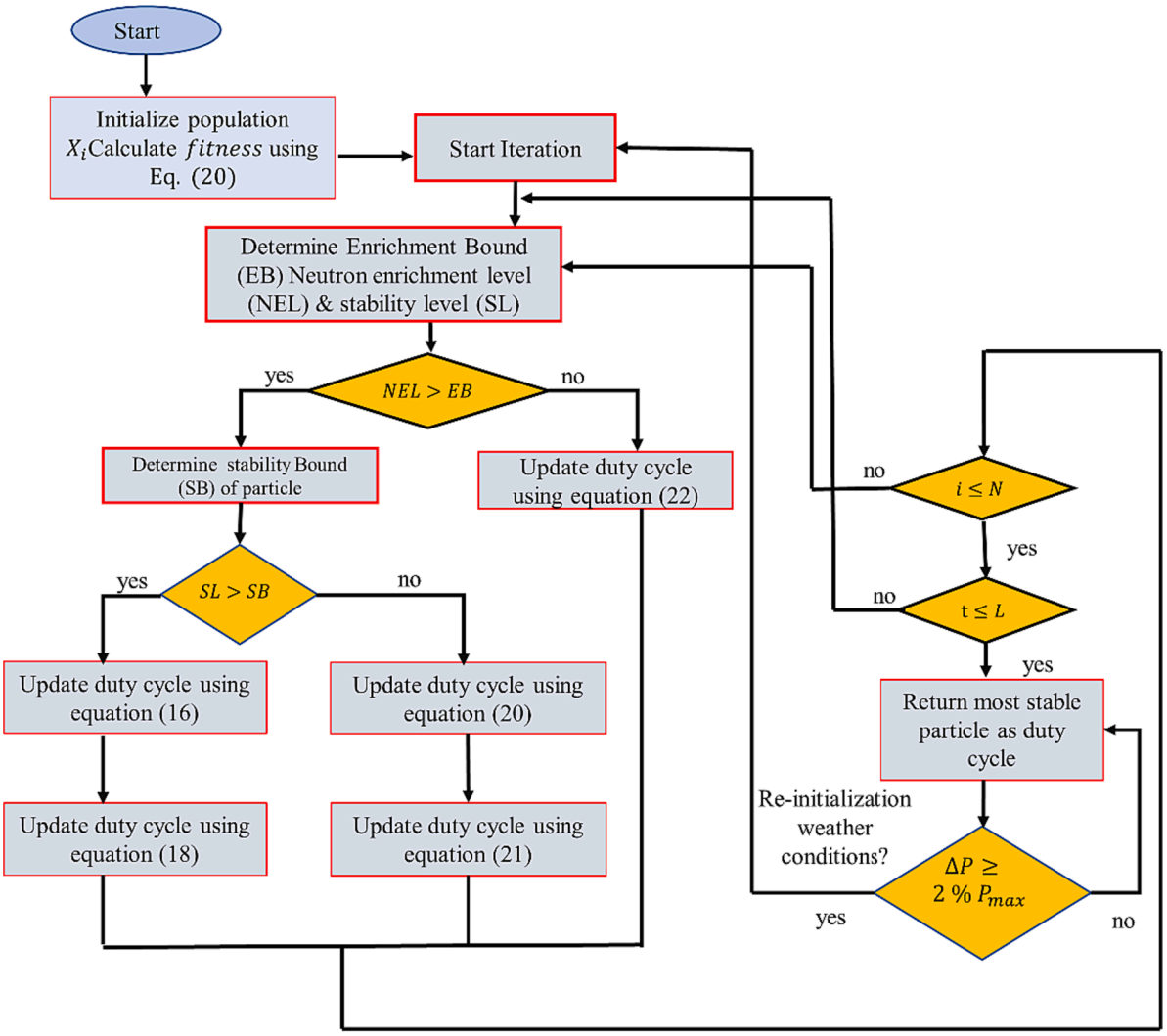

Fig. 6. The flowchart of EVO for MPPT tracking.

Initialize *random population z of control variables i.e., Duty cycle*
Initialize iteration counter t=0 & maximum iteration N
Evaluate fitness as Neutron Enrichment Level (NEL) using equation (22)
while $t < N$
Determine Enrichment Bound (EB) ;
Determine global best duty cycle based on stability level i.e.
for $(i = 1{:}n)$
Determine stability level (SL) and NEL of the i^{th}*particle*
if $(NEL_{,i} > EB)$
Determine stability bound (SB);
if $(SL_{,i} > SB)$
Update alpha index using equation (16).
Update gamma index using equation (18).
elseif $(SB \geq SL_{,i})$
Determine center of particles & neighboring particle using equations (20) & (21) ; ***end***
elseif $(EB \geq NEL_{,i})$
Update particle using equation (22); ***end***
end if
end if *;* ***end for***
t=t+1
end while
Return most stable particle as best duty cycle

Fig. 7. The pseudo code of EVO for MPPT tracking.

maximum number of iterations was set at 50. The second criterion is power change (ΔP). ΔP must be kept within $\leq$ 2% of the maximum rated power. The algorithm must be reinitialized due to the significant change in operational circumstances and weather. Fig. 6 and Fig. 7 show the logical flowchart and pseudo code respectively, for the EVO based MPPT.

3.2. Tracking mechanism

The duty cycle serves as the search space, and its range is 0 to 1. In the search space, four particles named Pa_1, Pa_2, Pa_3, and Pa_4 are initialized. Variable V_{Pa_i} contains the voltage search range (min, max) for particle Pa_i (i = 1, 2, N). Eq. (37) explains how the best particle was chosen.

$$V_{Pa\_best(n)} = gbest(V_{Pa_{best(1)}}, V_{Pa\_best(2)}, V_{Pa\_best(3)}, V_{Pa\_best(4)} \quad (23)$$

The reference voltage calculated by EVO is displayed in Fig. 8. The repeated movement of particles is shown in Fig. 9 (a–f). Smoother shifts are achieved which results in stable power transient without random oscillations. It is also observed that the maximum exploration of search space is done by the proposed EVO ranging from 15 to 200 V on the x-axis. Initially, the population shifts towards the opposite end because of higher average weight. The EVO computes the reference voltages up to 175 V. Fig. 9 suggests that initially *pace* is very high and reduction is *pace* limits the range of EVO particles in final iterations.

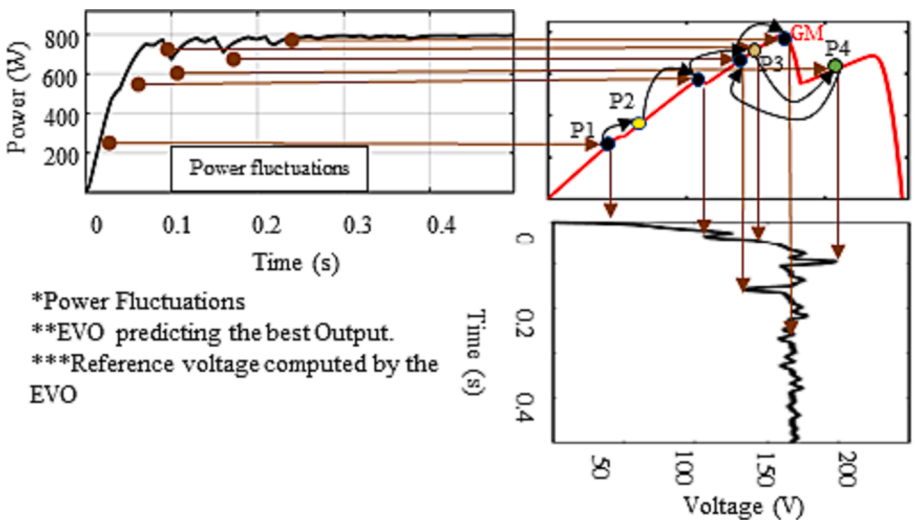

Fig. 8. EVO GM tracking on P-V curves with respect to output power and reference voltage.

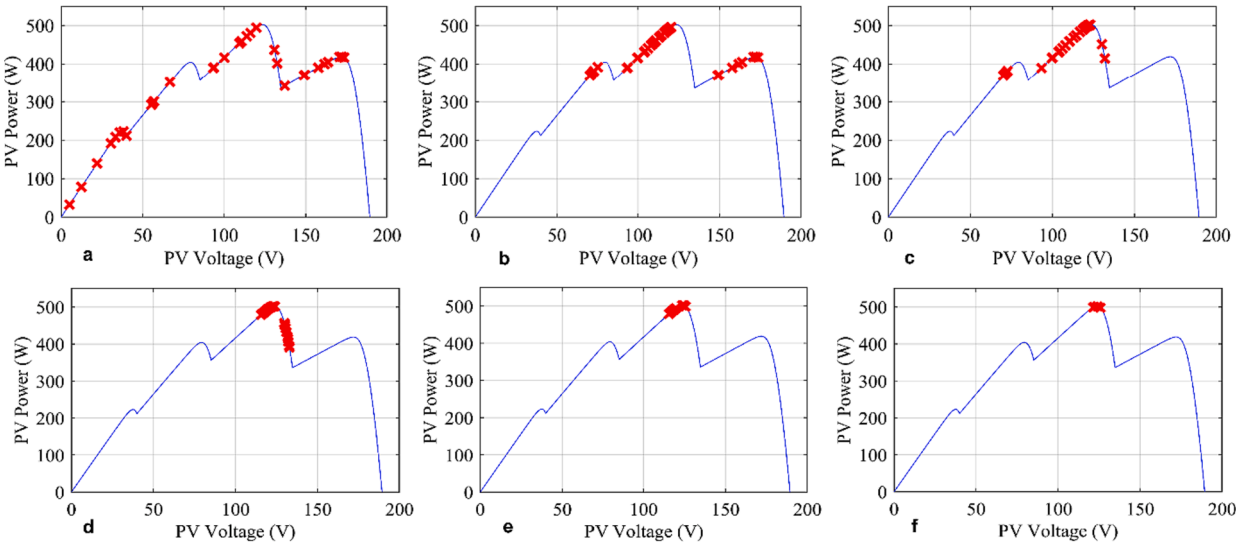

Fig. 9. EVO iterative behavior during GM search on P-V curve.

4. Results and discussion

In this section, a detailed study of results will be made. Thorough comparison of optimized P&O, PSO [31], WOA [31] and CSA [32] is made with proposed EVO. The problem is formulated using five case studies which includes temperature, irradiance, PS, CPS and field atmospheric data study. Case 1 deals with fast varying irradiance that occurs due to moving clouds, shade and dust accumulation. Case 2 deals with the varying temperature typically encountered by PV systems throughout the day. Case 3 is a classical partial shading condition problem and case 4 is built upon complex partial shading condition. The case 5 represents real world application scenario in which the energy harvest is examined through 24-hour operation of MPPT controller. The seven quantitative matrices i.e., tracking time (TT), settling time (ST), % age efficiency, MPP, average power etc. and 3 statistical matrices i.e., MAE, RE, and RMSE are used to compare the performance of the competing approaches.

4.1. Case 1 fast change in irradiance

Moving cloud shadow, dust accumulation and angle of elevation of sun causes significant change in irradiance levels throughout the day [33]. The output of the PV system degrades significantly and MPP swings due to these irradiance changes. The change in irradiance has dominant effect upon current generation and relatively low effect upon the voltage drop [34]. In this case, two distinct transitions in irradiance are considered after every 2 s as shown in Table 3. At STC condition the irradiance is 1000 W/m^2 and T = 25 °C. The irradiance drops from 1 kW/m^2 to 0.450 kW/m^2 rises to 0.650 kW/m^2. The maximum power is 1201.2 W, 545.2 W and 788 W, respectively and the relative average power is 844.8 W.

Table 3
Fast changing irradiance pattern for Case 1.

Case No. & Description	Irradiance pattern $G\frac{kW}{m^2}\times 1000$				$P_{max}(W)$
	PV_1	PV_2	PV_3	PV_4	
Case1: Fast Vary. Irradiance	1,0.45, 0.65	1,0.45, 0.65	1,0.45, 0.65	1,0.45, 0.65	1201,545,778

The power transient is compared in Fig. 10 (a) The duty cycle

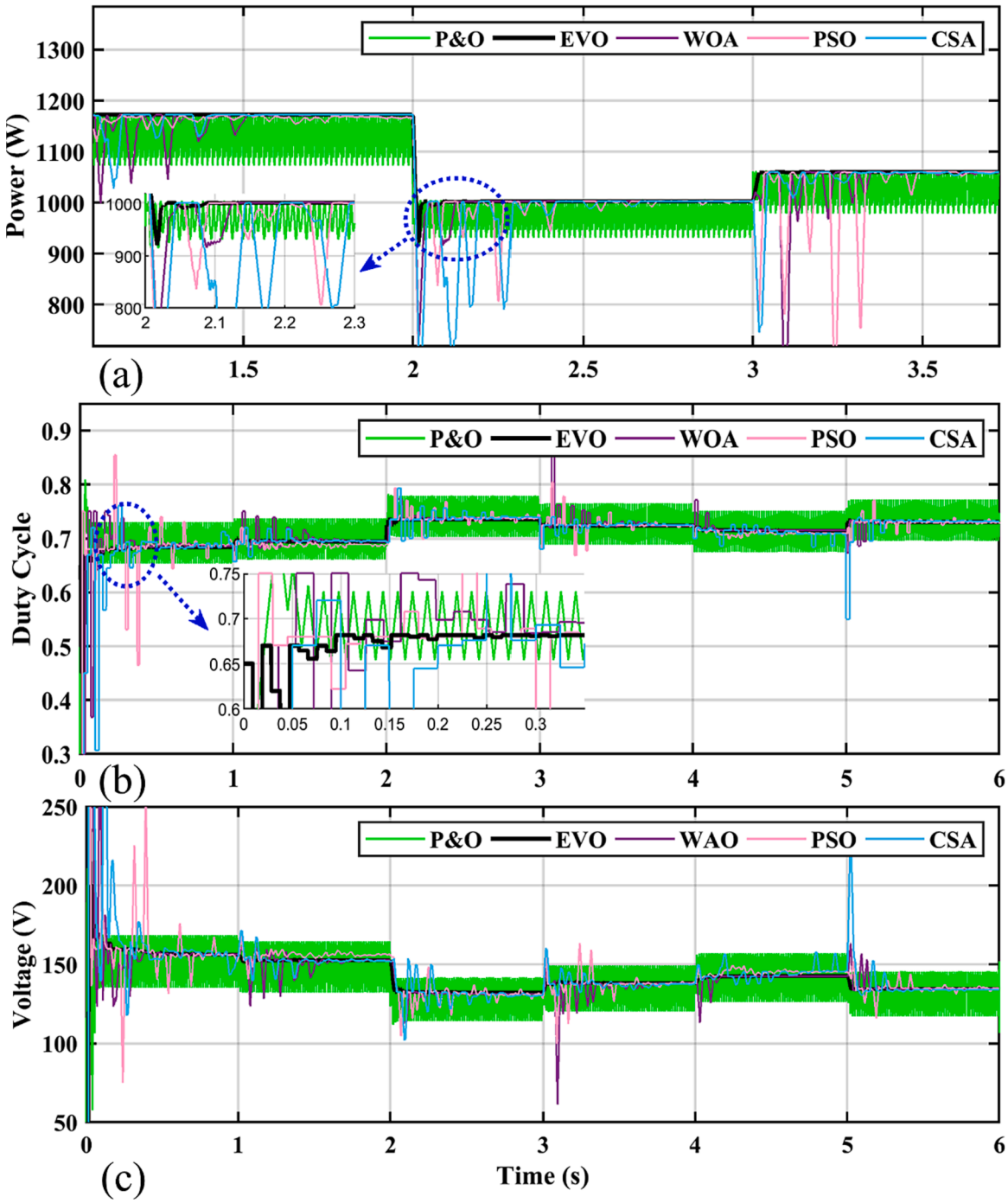

Fig. 10. (a) Power variations for case 1 (b) Duty cycle variations for case 1 (c) Voltage variations for case 1.

comparison is presented in Fig. 12. In the interval 0–2 s, EVO achieved the highest efficiency reaching 1201 W followed by WOA 1198.4 W, PSO 1198.3 W and CSA 1197.4 W and P&O is 1176 W. The proposed EVO achieves 99.99 % power convergence efficiency followed by WOA 99.75 %, PSO 99.71 %, CSA 99.71 % and P&O 98 %.

During the duration of 0–6 s, highest average power is achieved by EVO at 832 W followed by WOA 806 W, P&O 819 W, PSO 801 W and CSA 799 W. Relatively EVO produced 13–33 W more power which translates in up to 4 % more average power and energy harvest due to effective tracking of MPP by the proposed techniques. According to the power dynamics, the performance under fast varying irradiance is EVO > WOA > PSO > P&O > CSA.

The proposed EVO achieve a tacking time (TT) of 120 ms. Interestingly the P&O tracks the GM within 120 ms but failed to settle. WOA, CSA and PSO take 360 ms, 360 ms and 340 ms respectively. The ST of EVO is 160 ms. PSO and CSA has longest settled time of 850 and 830 ms and WOA settles within 435 ms. The duty cycle variation is shown in Fig. 10 (b). The proposed EVO is 42–53.5 % faster. The PSO and CSA take up to 30 iterative cycles to settle at GM while EVO takes less than 17 iterations. The P&O follows GM and generates continuous oscillations at 24 W. In Fig. 10 (c) voltage variations are shown.

4.2. *Case 2: Fast temperature variations*

This case addresses the rapidly fluctuating temperature. The output voltage has a significant impact on voltage drop and is inversely

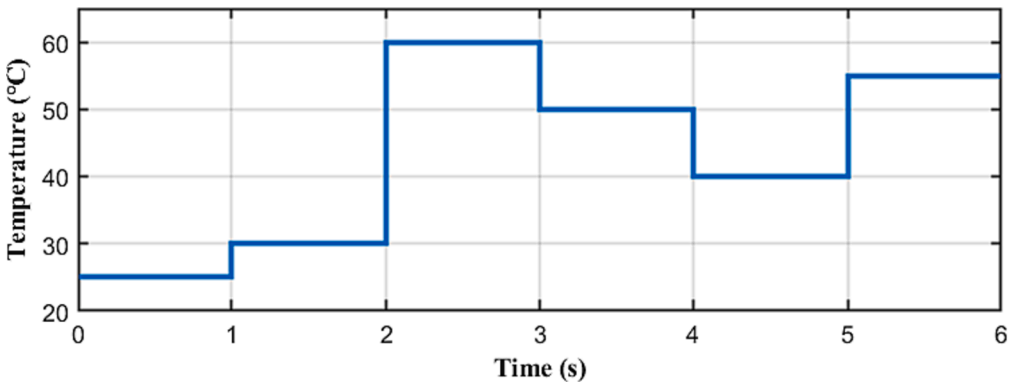

Fig. 11. Time varying temperature condition of Case 2 for the PV system.

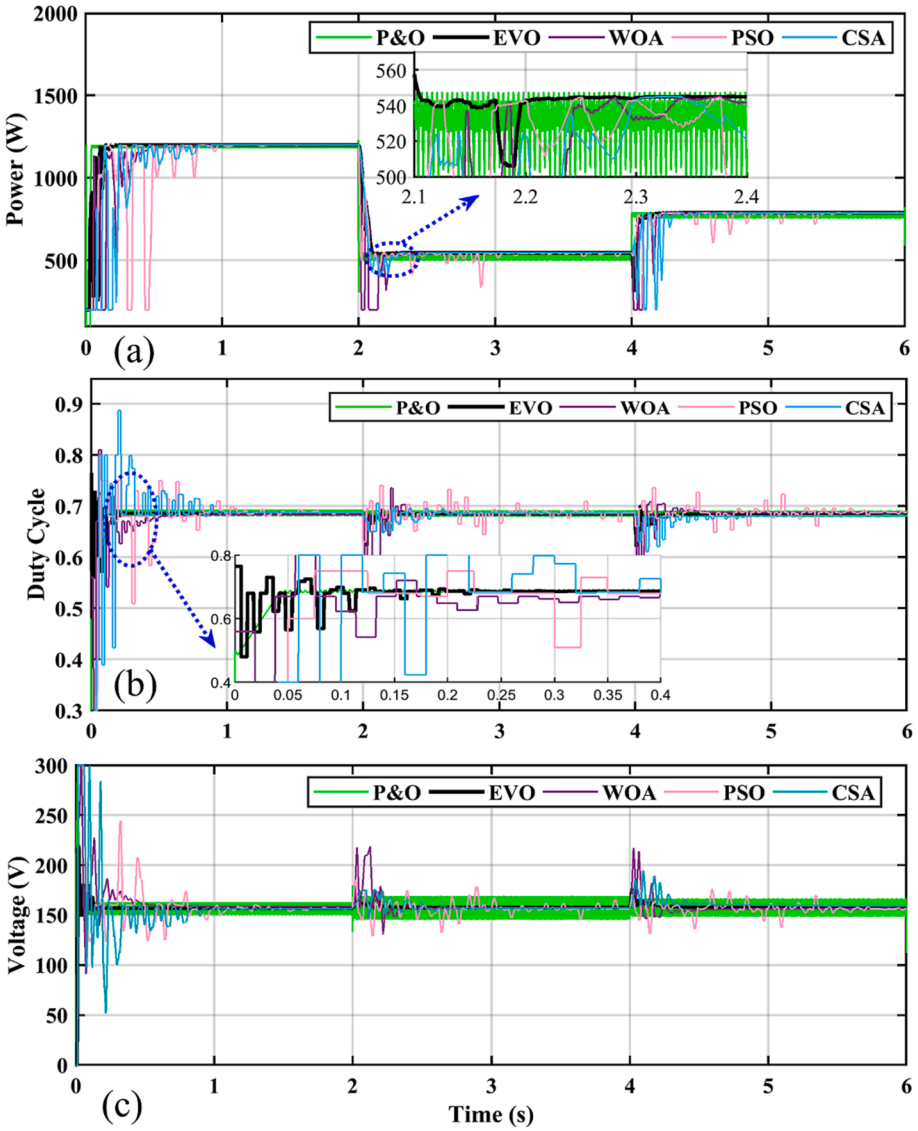

Fig. 12. (a) Power comparison for case 2 (b) Duty cycle comparison for case 2 (c) Voltage comparison for case 2.

proportional to operational temperature [35]. Fig. 11 displays the test pattern at G = 1000 W/m2. The Case 2 temperature pattern starts at 25 °C and transitions occurs every second.

Fig. 12 (a) & (b) show the comparison of power & the duty cycle, respectively. With a 99.99 % efficiency, EVO achieves the highest power of 1201 W, followed by WOA at 1199 W, CSA at 1197 W, PSO at 1189 W, and P&O at 1188 W, with respective efficiency ratings of 99.99 %, 99.71 %, 99.75 %, and 98.0 %. A higher mean average indicates the robustness of the controller in the transient phase of operation. Average power is a better indicator of performance analysis. The EVO achieved average

Table 4
Irradiance levels to generate partial shading for case 3.

Case No.	Irradiance $G_i(\frac{kW}{m^2}) \times 1000$				P_{max} (W)
Case3 PS	PV_1 0.79	PV_2 0.66	PV_3 0.52	PV_4 0.31	500

power of 1082 W, PSO 1060 W, WOA 1059 W, CSA 1050 W and P&O is at 1050 W. The proposed EVO achieve 2–3 % more average power.

According to the findings in Fig. 12 (c), EVO has shortest TT & ST of 120 ms and 130 ms respectively. Despite the fact that Pert & Observe algorithm needs only 100 ms to track the GM, it results in power loss owing to random oscillations. The WOA, CSA, and PSO have TT of 290 ms, 360 ms, and 370 ms with ST of 350 ms, 420 ms, and 740 ms respectively. The sequence of performance is EVO > WOA > CSA > PSO > P&O.

4.3. Case 3 partial shading problem

Major problems with solar electric generation are brought on by the PS [36,37]. The production capacity of a PV panel may be reduced up to 70 % by a 10 % shadow. Different irradiance levels result in varying voltages and currents. The least productive panels create a hotspot effect. The power is lost as heat energy, which could harm PV panels that are serving as a resistive load [38].

For a 4x1 PV array, Table 4 offers the partial shading pattern. Figs. 5 and 6 display the P-V and I-V curves. The P-V curves illustrates 4 MPPs with 3 LM and 1 GM. GM is centralized. The power at LM1 = 238 W, LM2 = 440 W, LM3 = 455 W and GM lies at 500 W.

Results for power transients are illustrated in Fig. 13 (a), and duty cycle control is depicted in Fig. 13 (b). EVO, WOA, PSO, CSA, and P&O each achieved a maximum power of 500 W, 499.7 W, 499.3 W, 499.2 W, and 440 W under PS conditions, respectively. The respective efficiencies

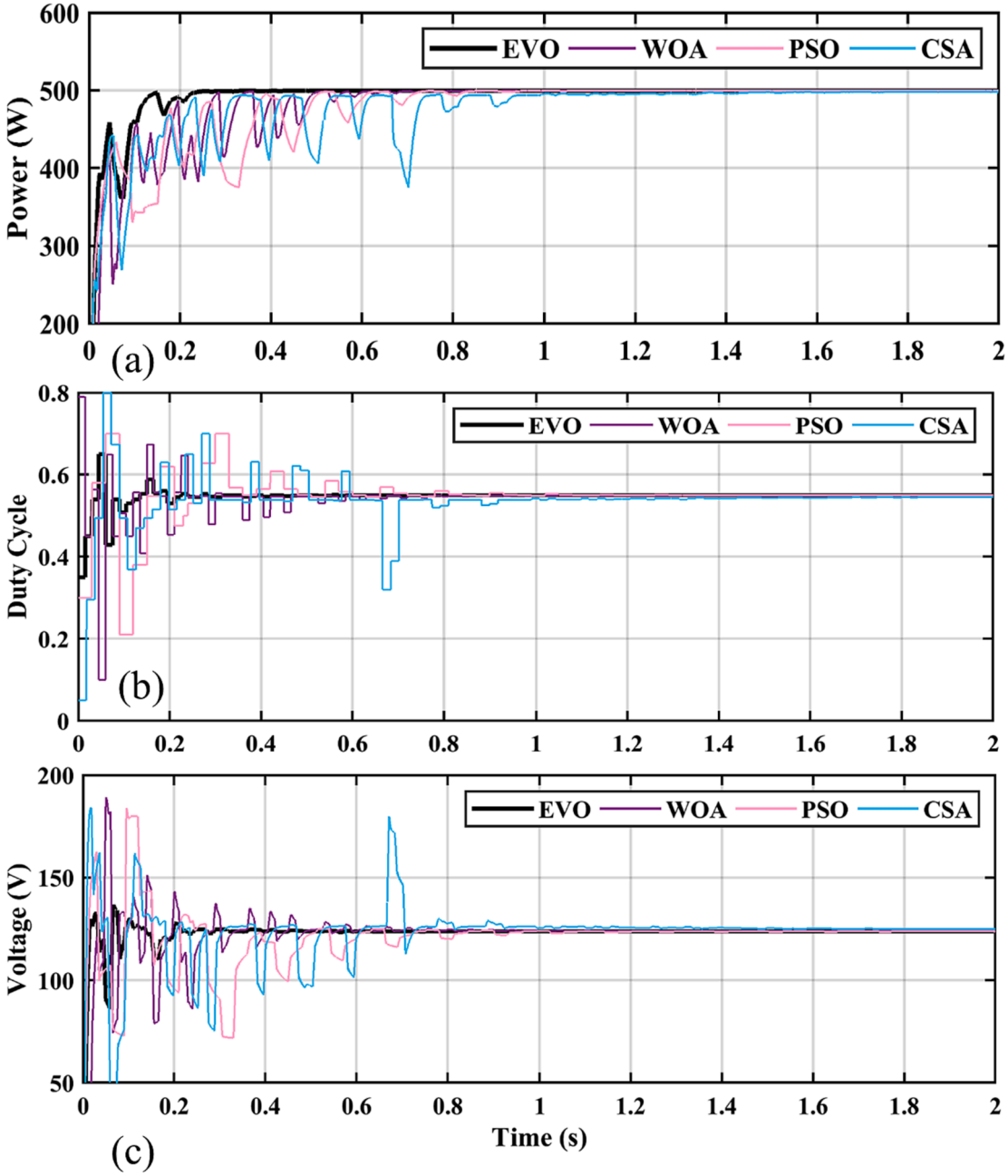

Fig. 13. (a) Power comparison for case 3 (b) Duty cycle comparison for case 3 (c) Voltage comparison for case 3.

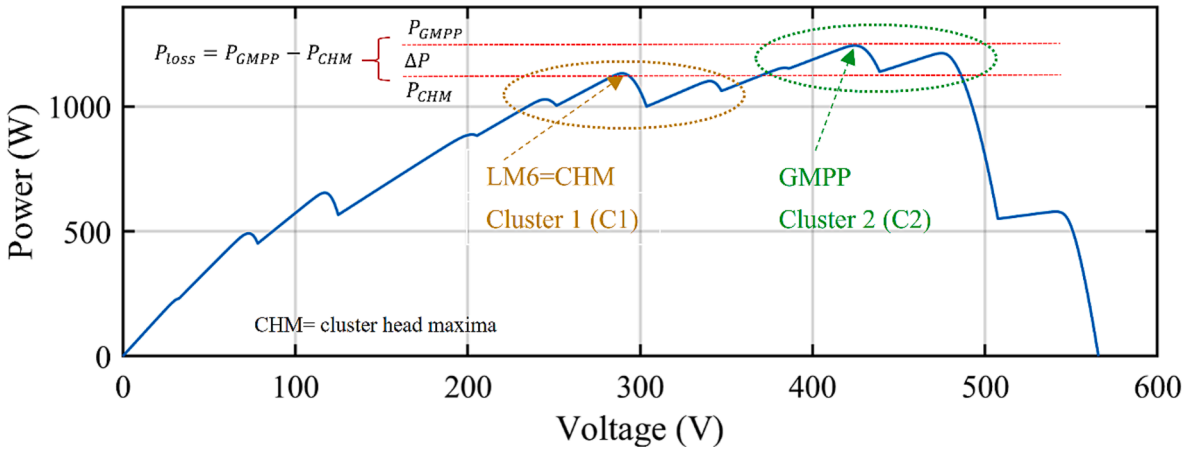

Fig. 14. The cluster formation due to complex partial shading conditions.

Table 5
Irradiance levels to generate complex partial shading for case 3.

Case No.	Irradiance $G_i(\frac{kW}{m^2})$			P_{max}(W)
Case 4 CPS	Module1 = 385	Module5 = 555	Module9 = 515	1243
	Module2 = 140	Module6 = 425	Module10 = 395	
	Module3 = 985	Module7 = 585	Module11 = 740	
	Module4 = 585	Module8 = 335	Module12 = 910	

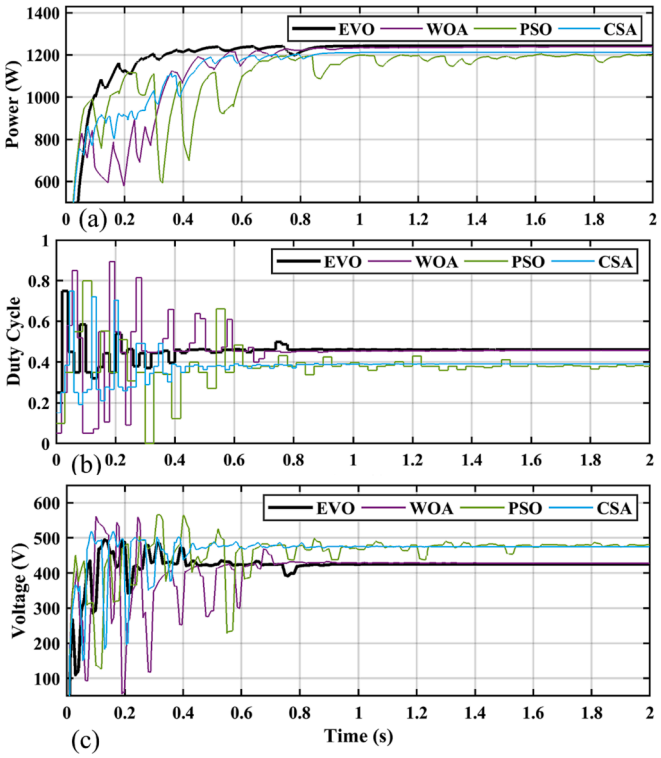

Fig. 15. (a) Power comparison for case 4 (b) Duty cycle comparison for case 4 (c) Voltage comparison for case 1.

of EVO, WOA, PSO, CSA, and P&O are 100 %, 99.86 %, 99.75 %, 99.31 %, and 88 % respectively.

EVO achieves the highest average power of 491 W, followed by WOA at 477 W, PSO at 475 W, CSA at 474 W, and P&O at 381 W. The ST of EVO is 250 ms, and it can take up to 200 ms to track GM. The EVO shows 52.3 % faster TT and 80.72 % quicker ST with respect to CSA. The P&O has fast-tracking under STC conditions taking as low as 100 ms but suffers from LM trap and unable to settle at GM. Results show that, the EVO track the GM in 12 iterations, and in 20 iterations, it reaches MPP. EVO > WOA > PSO > CSA > P&O is a succinct way to describe case 3 performance. Voltage variations with stable output are shown in Fig. 13 (c).

4.4. Case 4: Complex partial shading conditions

The complex partial shading (CPS) occurs due to comprehensive PS of numerous PV arrays [39,40]. As a result, several closely associated MPP are formed on the P-V curves [40]. Fig. 14 shows the cluster formation in two group of closely packed LM. Each cluster has three MPP. Table 5 provides the irradiance pattern for 12x1 PV array.

In total 11 local maxima are named LM_i for $(i = 1, 2, \cdots, p)$, and $p \leq 11$. The LMP from left to right are 223.3 W, 490 W, 634.8 W, 887 W, 1028 W, 1123 W, 1102 W, 1155 W, 1243 W, 1218 W, and 578.8 W respectively. The first cluster (C1) contains LM_{5-7} with average power of 1.0109×10^3 . The second cluster (C2) contains LM_{8-10} with average power of 1.0362×10^3. The power is compared in Fig. 15 (a). The duty cycle comparison is shown in Fig. 15 (b).

The EVO, WOA, CSA, and PSO tracked the GMPP in 260 ms, 530 ms, 540 ms, and 740 ms respectively. The algorithms then took 490 ms, 730 ms, 720 ms and 1.13 ms to settle without oscillations. The PSO exhibits the biggest variations in power transients, as seen in Fig. 15 (c). The TT of EVO is 66.7 % faster than PSO's, followed by CSA at 56 % and GHO at 50.9 %. In this case, the overall performance order is EVO > WOA > CSA > PSO > P&O. The quantitative comparison for all the four cases is presented in Table 6.

4.5. Case 5: Real world data

In this case, the suggested MPPT controller viability and efficacy are assessed by using the field atmospheric data. The moving clouds, temperature variance, and regional seasons are the factors that determine the efficiency of the installed PV system [41]. The China Meteorological Agency (CMA) has information on total direct irradiance. The weather profile of average seasonal days is produced using the data in Fig. 16. It is warm and sparkling throughout the summer and spring. The winter season is the least productive, whereas fall is likely to have lower irradiance exposure. The data transients are sampled every five minutes for a duration of 24 h.

Location of Beijing is 39.9042oN/116.4074oE. The irradiance profile of Beijing is shown in Fig. 16 (a), and the solar energy available year-round for various installation angles is shown in Fig. 16 (b). The

Table 6
Quantitative comparison of EVO with WOA, PSO, CSA and P&O.

Tech. Name	Case	Converge Time(s)	Settling Time(s)	Power at GM (W)	Avg. Power	Max Power tracked (W)	Harvested Energy (W)	Efficiency(%)
EVO	Case1	0.12	0.16	1201	832	1201	1.664×10^3	99.99
	Case2	0.12	0.13	1201	1082	1201	2.164×10^3	99.99
	Case3	0.21	0.24	500	491	500	0.982×10^3	99.99
	Case4	0.26	0.49	1242.2	1188	1243	2.376×10^3	99.94
WOA	Case1	0.36	0.43	1201	806	1198.4	1.612×10^3	99.75
	Case 2	0.29	0.35	1201	1059	1199	2.119×10^3	99.80
	Case 3	0.37	0.57	499.7	477	499.7	0.954×10^3	99.90
	Case 4	0.53	0.73	1238	1136	1239	2.272×10^3	99.6
PSO	Case 1	0.34	0.85	1201	801	1198.3	1.602×10^3	99.71
	Case 2	0.36	0.74	1201	1060	1198	2.120×10^3	99.75
	Case 3	0.52	0.73	499.3	475	499.3	0.950×10^3	97.69
	Case 4	0.74	1.13	1204	1100	1205(LM)	2.200×10^3	96.94
CSA	Case 1	0.36	0.83	1201	799	1197	1.598×10^3	99.71
	Case 2	0.37	0.42	1201	1050	1197.4	2.100×10^3	99.71
	Case 3	0.42	0.86	499.2	474	499.2	0.948×10^3	99.31
	Case 4	0.54	0.72	1212	1131	1213(LM)	2.262×10^3	97.52
P&O	Case 1	0.12	0.12	1201	819	1176	1.638×10^3	98.00
	Case 2	0.12	0.12	1201	1050	1188	2.100×10^3	98.00
	Case 3	0.13	–	440	381	440(LM)	0.800×10^3	88.00
	Case 4	0.21	–	–	–	LM	LM	LM

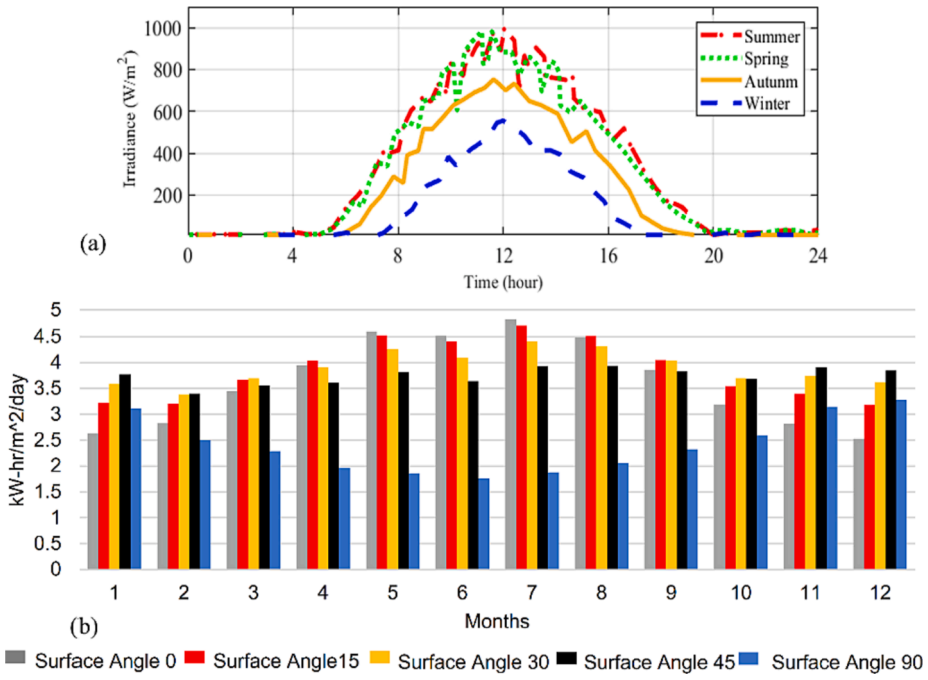

Fig. 16. Weather irradiance profile of Beijing city (a) 24-hour irradiance for Winter, Summer, Spring & Autumn (b) average irradiance for one month considering various surface angles.

average irradiance is 3821 W/m2, and the direct normal irradiance is 3930 W/m2. The annual mean temperature is 32.1 °C, with high temperatures of 39.3 °C and lowest temperatures of −12.8 °C. The average amount of power available between 10:00 and 15:00 is 820 W. Average peak power throughout the summer and fall is 897.2 W and 811 W, respectively. Winter and fall are the months when solar energy is least abundant. Table 7 provides a summary of the findings.

The power and energy harvest for the summer season are shown in Fig. 17 & Fig. 18. The maximum power of 1192 W is achieved by EVO followed by WOA at 1190 W, PSO at 1178 W, CSA at 1172 W, and P&O at 1168 W. The energy harvested during 24 h is 13.3KWh, 13.22KWh, 13.07KWh, 13.0KWh, and 12.58KWh, respectively. The proposed technique produces up to 5 % more energy.

The power and energy harvest for the spring season are shown in Fig. 19 and Fig. 20. The maximum peak power attained by EVO is 1182 W, WOA 1170 W, PSO 1143, CSA 1168WW, and P&O is 1144 W. The hourly mean power for EVO, WOA, CSA, PSO and P&O is 498 W, 492.3 W, 487.3 W, 480.3 W, and 474.8 W respectively. The total energy harvested by EVO is 11.95kWh. The EVO has 105 % more energy. WOA and CSA achieve higher peak power, still WOA has a higher average due to its effective tracking. Higher energy harvest improvises the techno-economic feasibility and life cycle cost (LCC) of the PV system installations.

4.6. *Experimental verification*

The primary objective of this section is to implement the Maximum Power Point Tracking (MPPT) controller model onto a physically

Table 7
The comparative 24 h results for case 5.

City	Season	Measure	EVO	WOA	PSO	CSA	P&O
Beijing	Summer	Peak power (W)	1192	1190	1178	1172	1168
		Mean Power (W)	554	550.9	544.4	541.6	524.0
		Energy Harvest (kWh)	13.3	13.22	13.07	13.0	12.58
	Spring	Peak power (W)	1182	1170	1143	1168	1144
		Mean Power (W)	498	492.2	480.3	487.3	474.8
		Energy (kWh)	11.95	11.82	11.53	11.60	11.38

embedded processor and subsequently conduct a closed-loop simulation using a simulated plant model. This integration and simulation process is commonly referred to as the "processor-in-the-loop" (PIL) test. During the PIL test, the EVO-MPPT controller is substituted by a PIL block, where the controller code is executed on the actual hardware of the embedded processor. This setup allows us to validate the effectiveness of the proposed MPPT control strategy on a real embedded board.

To accomplish this, the Arduino MKRZERO board is utilized as the embedded platform for conducting the PIL experimentation. The Arduino MKRZERO features an integrated Microchip Technology ATMEL SAMD21 microcontroller. This microcontroller is equipped with a powerful 32-bit Arm® Cortex®-M4F processor, which includes a Floating-Point Unit (FPU). The processor operates at speeds of up to 120 MHz, and it boasts 256kB of flash memory along with 32kB of SRAM. By executing the MPPT controller on the ARM Cortex-M4F processor of the Arduino MKRZERO board, we can thoroughly evaluate the capabilities of the processor in handling the complex computations involved in the MPPT algorithm. This process is crucial for verifying the feasibility of employing the developed MPPT control strategy in real-world applications on an embedded system.

Fig. 21 illustrates the embedded board, i.e., the Arduino MKRZERO board, which serves as the hardware platform for conducting the processor-in-the-loop (PIL) experiments. With this setup, we aim to ensure that the embedded processor effectively executes the MPPT controller and successfully regulates the power output to maximize the efficiency of the photovoltaic system under various conditions. The results from the PIL test will provide valuable insights into the performance and reliability of the MPPT control strategy on the chosen embedded board and microcontroller configuration.

The Processor-in-the-Loop (PIL) block, as shown in Fig. 21, is carefully constructed and integrated with the plant model to capture the photovoltaic (PV) output voltage and current. This integration enables the PIL block to implement the proposed algorithm, determining the necessary duty cycle required for optimum power point tracking. Subsequently, the PIL block sends this calculated duty cycle back to the plant model. The essence of the PIL process lies in its real-time testing capability. During the PIL test, the generated code of the MPPT controller is executed and tested in real-time on the chosen embedded processor (Arduino MKRZERO board), while the plant model continues to run on a computer. This configuration facilitates the identification and rectification of potential errors in the control algorithm, thus ensuring the reliability and accuracy of the MPPT control strategy.

Fig. 22 illustrates the outcome of the PIL test. It clearly exhibits the results obtained from this test and emphasizes their close similarity to the simulation results achieved using MATLAB/Simulink. This congruence between the PIL test and the simulation results validates the efficacy and correctness of the MPPT control algorithm proposed in this study.

The successful verification of the MPPT control algorithm on the real microcontroller (Arduino MKRZERO board) through the PIL test is a

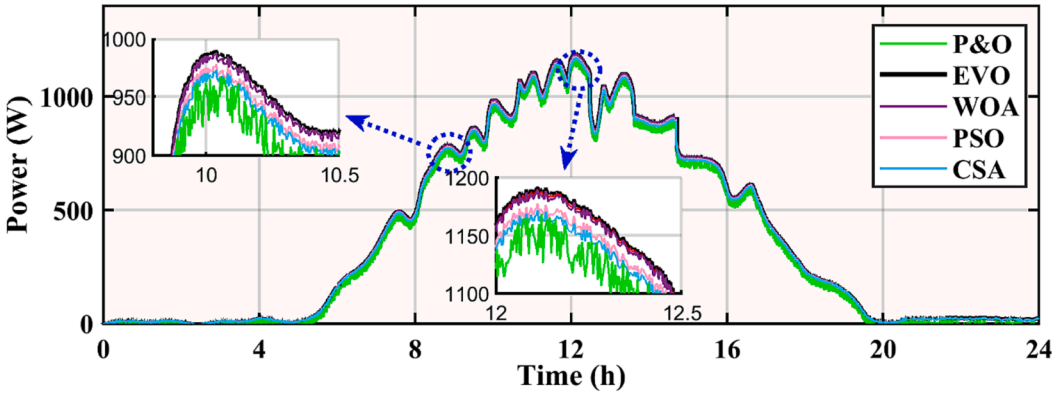

Fig. 17. Summer power comparison for case 5.

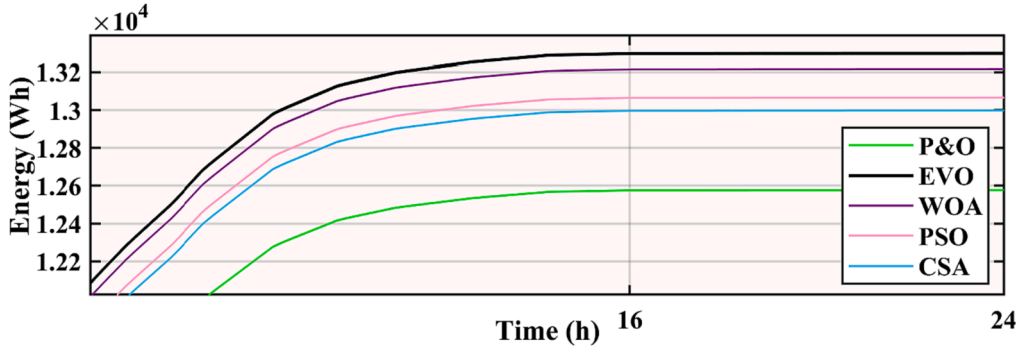

Fig. 18. Summer energy harvest comparison for case 5.

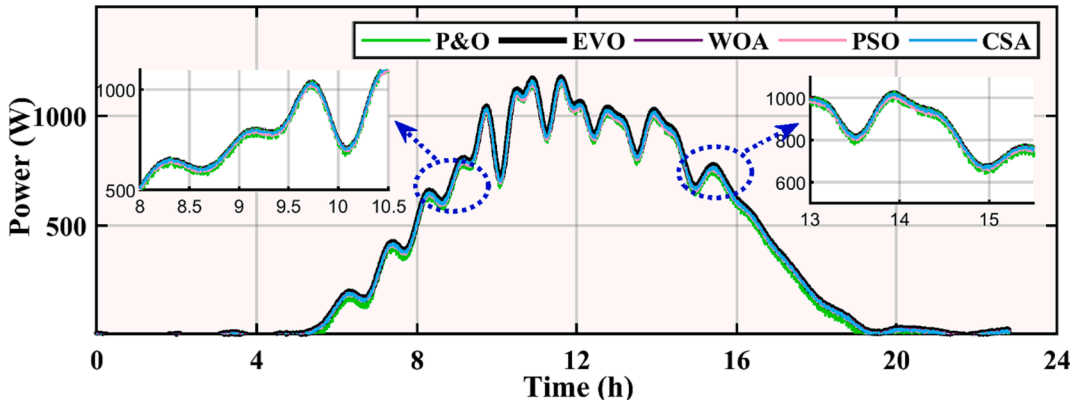

Fig. 19. Spring power comparison for case 5.

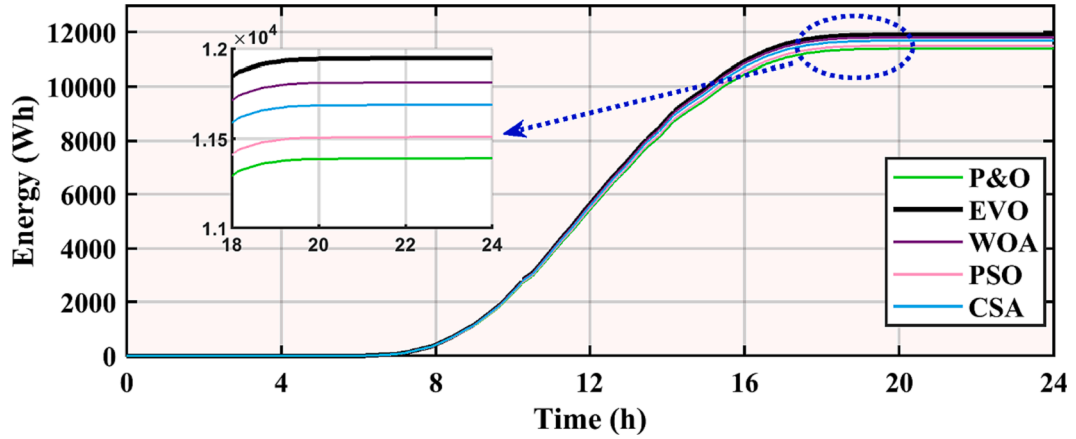

Fig. 20. Spring energy comparison for case 5.

critical milestone in this research. It demonstrates that the embedded processor can execute the developed algorithm in real-time and achieving accurate power tracking performance, which holds significant implications for practical applications of this control strategy in real-world PV systems.

By conducting the PIL test, we have effectively bridged the gap between simulation and real-world implementation. This process ensures that the proposed MPPT control algorithm functions as intended on the embedded board, offering the potential for enhanced energy harvesting efficiency in photovoltaic applications. The thorough validation of the algorithm's performance through the PIL test provides a solid foundation for confidently employing this control strategy in actual embedded systems, contributing to the advancement of renewable energy technologies.

In the PIL study, we evaluated the performance of EVO against PSO and Perturb and Observe algorithm. The MPPT control was tested under fast varying operating conditions, starting at 1000 $\frac{W}{m^2}$ and falling to 500 $\frac{W}{m^2}$ and again raised to 700 $\frac{W}{m^2}$ for 25 W $\pm$ 3 W Sonew flexible polycrystalline solar panel with 17 % efficiency in 4x2 configuration. Our findings demonstrate that the proposed EVO exhibits superior performance in terms of faster tracking time, higher power conversion efficiency, and reduced oscillations at power transition points. Specifically, during the sudden irradiance reduction at t = 2 s and t = 4 s. EVO efficiently tracked the global maximum (GM) within 130 ms and settled at the GM in 250 ms. On the other hand, PSO exhausts approximately 540 ms to track and an additional 260 ms to settle at the new maximum power point. P&O oscillations render its performance and are fluctuating the control signal causing unstable output power. Additionally, the magnitude of the fluctuations observed in EVO's power tracking was significantly smaller compared to PSO, as clearly illustrated in the zoomed view of the graphs. The power tracking efficiency of EVO was determined to be 99 %, indicating its capability to harvest more energy while producing fewer fluctuations.. EVO generated stable output despite minor noise caused by uncertain resistances and connection capacitances. At irradiance transition, the EVO can deal with reference voltage fluctuation by effectively generating updated reference voltage. PSO on the other hand is least effective.

5. Discussions

5.1. Tracking & settling time

The tracking time (TT) of the MPPT controller is the amount of time it took to find GM, and the settling time is the amount of time it took to converge on GM in the search space without oscillations. The fewest number of iterations with the lowest TT and ST are preferred. An effective MPPT controller should have the smallest possible time constraints. EVO achieves the highest ST and TT, followed by WOA, CSA, PSO, and P&O. On average, the suggested controller results in 40–60 % improvement.

5.2. Tracking efficiency

The most crucial feature of the MPPT controller is efficiency. The mean and maximum power efficiencies are investigated for all five cases. The proposed strategy outperforms the alternatives in both indices. The PSO and CSA's lack of efficiency in power tracking is revealed in cases 4 and 5.

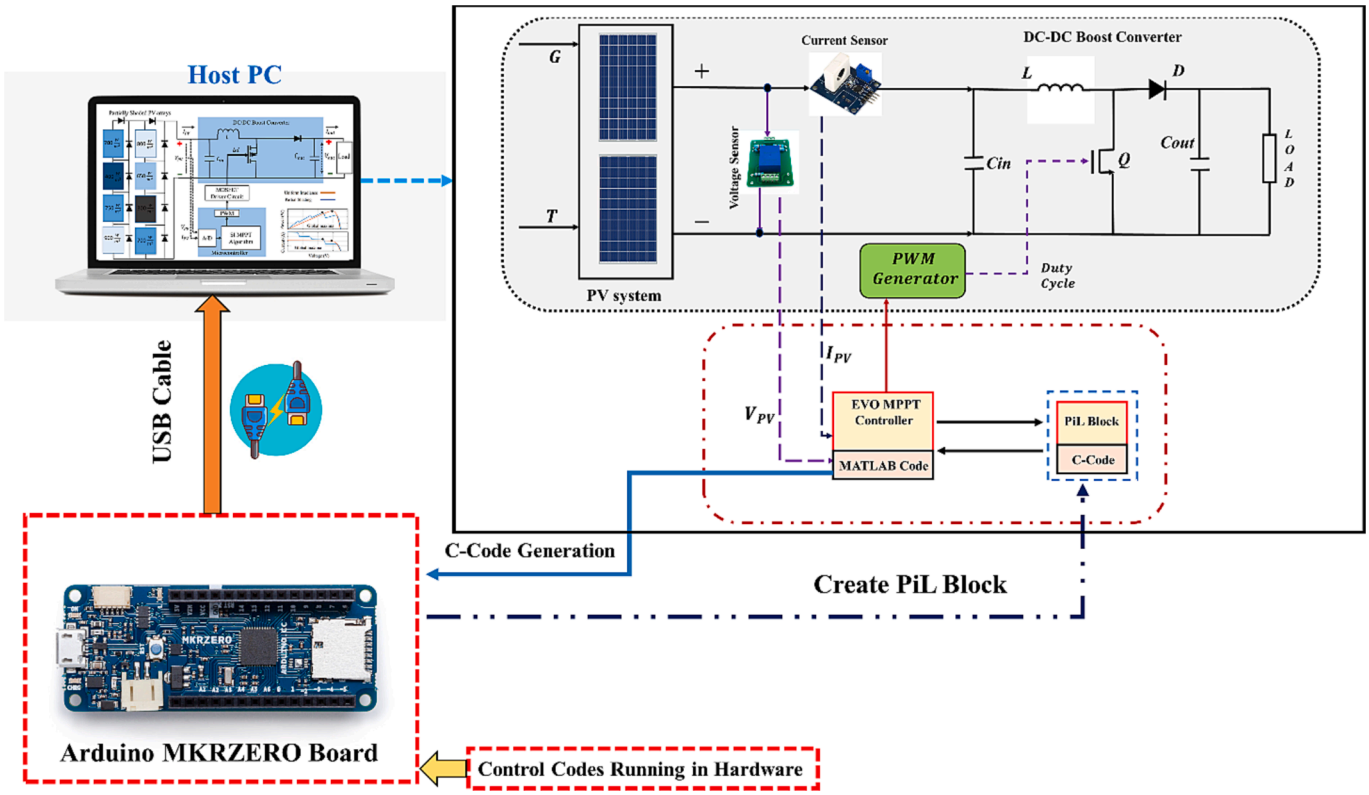

Fig. 21. Diagram of PV generation using PIL block.

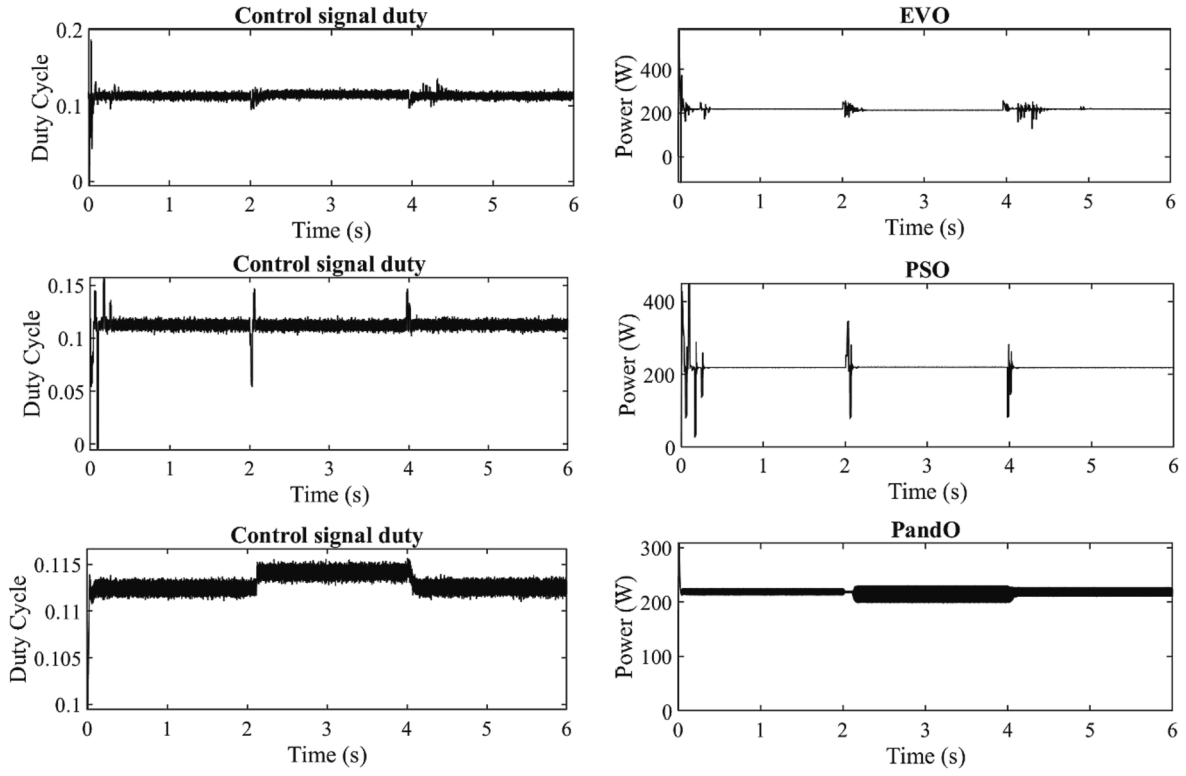

Fig. 22. PIL hardware experimental results comparison of EVO, PSO and P&O.

5.3. Oscillations and fluctuations

Voltage oscillations around MPP are a significant problem for conventional approaches. These oscillations should not occur. The results show that voltage and power oscillations have been successfully removed by the proposed technique. The results also show that for all

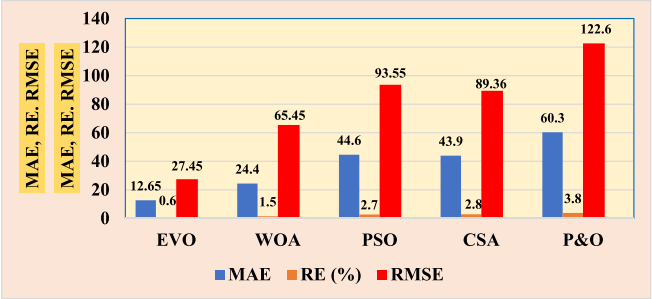

Fig. 23. Statistical analysis of the competing techniques.

five cases, the ripples remain ≤ 1 W.

5.4. Energy harvest

The highest energy is harvested by EVO. It is because of the robustness and overall performance superiority.

5.5. Statistical analysis

Mean absolute error (MAE),root mean square error (RMSE) and relative error are the indicators used to determine the sensitivity of competing techniques.

$$RE = \frac{\sum_{j=1}^{m}\left(P_{act,j} - P_{pv}\right)}{P_{pv}} * 100\% \tag{24}$$

$$MAE = \frac{\sum_{j=1}^{m}\left(P_{act,j} - P_{pv}\right)}{n} \tag{25}$$

$$RMSE = \sqrt{\frac{\sum_{j=1}^{m}\left(P_{act,j} - P_{pv}\right)^2}{n}} \tag{26}$$

where $P_{act,j}$ = actual output power in the j-th run, P_{pv} = max possible PV power, m = maximum runs. Compared to PSO, CSA,WOA, and P&O, the EVO produces lesser RE and MAE. The statistical analysis is presented in Fig. 23.

6. Conclusion

In order to address the issues of PS and delayed convergence in MPPT control, this research proposes a novel EVO based MPPT controller for the PV system. The superiority of the proposed EVO based MPPT controller is validated by comparing the results with highly optimized WOA, P&O, PSO, and CSA, under a variety of operating situations, including a field atmospheric data analysis, partial shading, complex partial shading and uniform shading conditions. The experimental, statistical and analytical study confirms the suggested EVO based MPPT controller's superior performance. The output oscillations are reduced to 1 W, and the power tracking efficiency reaches up to 99.99 %. When compared to traditional P&O, up to 12 % more power is produced, and when compared to contemporary MPPT controllers, tracking time improvements can be as much as 40–60 % faster. Overshoot, ripples, and fluctuations are all reduced to a minimum. Under field atmospheric conditions, EVO also produces great results. Finally, it can be concluded that under fast changing environmental conditions, the suggested EVO-MPPT strategy gives superior dynamic response, power conversion efficiency and tracking speed.

CRediT authorship contribution statement

Muhammad Kamran Khan: Conceptualization, Methodology, Resources, Project administration. **Muhammad Hamza Zafar:** Validation, Data curation. **Talha Riaz:** Investigation, Writing – original draft. **Majad Mansoor:** Data curation, Investigation, Validation. **Naureen Akhtar:** Funding acquisition, Investigation, Supervision, Validation, Writing – review & editing.

Declaration of Competing Interest

The authors declare that they have no known competing financial interests or personal relationships that could have appeared to influence the work reported in this paper.

Data availability

No data was used for the research described in the article.

References

[1] Okoye CO, Oranekwu-Okoye BC. Economic feasibility of solar PV system for rural electrification in Sub-Sahara Africa. Renew Sustain Energy Rev 2018;82:2537–47. https://doi.org/10.1016/j.rser.2017.09.054.
[2] Lee J, Shepley MM. Benefits of solar photovoltaic systems for low-income families in social housing of Korea: Renewable energy applications as solutions to energy poverty. J Build Eng 2020;28:101016. https://doi.org/10.1016/j.jobe.2019.101016.
[3] Petkov M, Markova D, Platikanov S. Modeling of electrical characteristics of photovoltaic power supply sources. IFAC Proc Vol 2006;39(19):183–8. https://doi.org/10.3182/20061002-4-BG-4905.00031.
[4] Escobar G, Pettersson S, Ho CNM, Rico-Camacho R. Multisampling maximum power point tracker (MS-MPPT) to compensate irradiance and temperature changes. IEEE Trans Sustainable Energy 2017;8(3):1096–105.
[5] Mohapatra A, Nayak B, Das P, Mohanty KB. A review on MPPT techniques of PV system under partial shading condition. Renew Sustain Energy Rev 2017;80:854–67. https://doi.org/10.1016/j.rser.2017.05.083.
[6] Rezk H, Fathy A, Abdelaziz AY. A comparison of different global MPPT techniques based on meta-heuristic algorithms for photovoltaic system subjected to partial shading conditions. Renew Sustain Energy Rev 2017;74:377–86. https://doi.org/10.1016/j.rser.2017.02.051.
[7] Saravanan S, Babu NR. Performance analysis of boost & Cuk converter in MPPT based PV system. In: 2015 International Conference on Circuits, Power and Computing Technologies [ICCPCT-2015], 19-20 March 2015; 2015. p. 1–6. https://doi.org/10.1109/ICCPCT.2015.7159425.
[8] Bendib B, Belmili H, Krim F. A survey of the most used MPPT methods: Conventional and advanced algorithms applied for photovoltaic systems. Renew Sustain Energy Rev 2015;45:637–48. https://doi.org/10.1016/j.rser.2015.02.009.
[9] Sarvi M, Azadian A. A comprehensive review and classified comparison of MPPT algorithms in PV systems. Energy Syst 2022;13(2):281–320.
[10] Sridhar R, Jeevananathan D, ThamizhSelvan N, Banerjee S. Modeling of PV array and performance enhancement by MPPT algorithm. Int J Computer Appl 2010;7(5):0975–8887.
[11] Bahari MI, Tarassodi P, Naeini YM, Khalilabad AK, Shirazi P. Modeling and simulation of hill climbing MPPT algorithm for photovoltaic application. In: 2016 International Symposium on Power Electronics, Electrical Drives, Automation and Motion (SPEEDAM), 22-24 June 2016; 2016. https://doi.org/10.1109/SPEEDAM.2016.7525990.
[12] Tey KS, Mekhilef S. Modified incremental conductance MPPT algorithm to mitigate inaccurate responses under fast-changing solar irradiation level. Sol Energy 2014;101:333–42. https://doi.org/10.1016/j.solener.2014.01.003.
[13] Bounechba H, Bouzid A, Snani H, Lashab A. Real time simulation of MPPT algorithms for PV energy system. Int J Electr Power Energy Syst 2016;83:67–78. https://doi.org/10.1016/j.ijepes.2016.03.041.
[14] Yap KY, Sarimuthu CR, Lim J-M-Y. Artificial intelligence based MPPT techniques for solar power system: A review. J Mod Power Syst Clean Energy 2020;8(6):1043–59.
[15] Seyedmahmoudian M, et al. State of the art artificial intelligence-based MPPT techniques for mitigating partial shading effects on PV systems–A review. Renew Sustain Energy Rev 2016;64:435–55.
[16] Mishra VL, Chauhan YK, Verma KS. A critical review on advanced reconfigured models and metaheuristics-based MPPT to address complex shadings of solar array. Energ Conver Manage 2022;269:116099. https://doi.org/10.1016/j.enconman.2022.116099.
[17] Pal RS, Mukherjee V. Metaheuristic based comparative MPPT methods for photovoltaic technology under partial shading condition. Energy 2020;212:118592. https://doi.org/10.1016/j.energy.2020.118592.
[18] Hamza Zafar M, et al. A novel meta-heuristic optimization algorithm based MPPT control technique for PV systems under complex partial shading condition. Sustainable Energy Technol Assess 2021;47:101367. https://doi.org/10.1016/j.seta.2021.101367.
[19] Mendez-Flores E, Ortiz A, Macias I, Molina A. Experimental Validation of an Enhanced MPPT Algorithm and an Optimal DC–DC Converter Design Powered by Metaheuristic Optimization for PV Systems. Energies 2022;15(21):8043 [Online]. Available: https://www.mdpi.com/1996-1073/15/21/8043.

[20] Aguila-Leon J, Vargas-Salgado C, Chiñas-Palacios C, Díaz-Bello D. Solar photovoltaic Maximum Power Point Tracking controller optimization using Grey Wolf Optimizer: A performance comparison between bio-inspired and traditional algorithms. Expert Syst Appl 2023;211:118700. https://doi.org/10.1016/j.eswa.2022.118700.
[21] Subramanian A, Raman J. Grasshopper optimization algorithm tuned maximum power point tracking for solar photovoltaic systems. J Ambient Intell Hum Comput 2021;12:8637–45.
[22] Eltamaly AM. A novel musical chairs algorithm applied for MPPT of PV systems. Renew Sustain Energy Rev 2021;146:111135. https://doi.org/10.1016/j.rser.2021.111135.
[23] Kamran Khan M, Hamza Zafar M, Mansoor M, Feroz Mirza A, Amir Khan U, Mujeeb Khan N. Green energy extraction for sustainable development: A novel MPPT technique for hybrid PV-TEG system. Sustainable Energy Technol Assess 2022;53:102388. https://doi.org/10.1016/j.seta.2022.102388.
[24] Hai T, Zhou J, Muranaka K. An efficient fuzzy-logic based MPPT controller for grid-connected PV systems by farmland fertility optimization algorithm. Optik 2022;267:169636.
[25] Kishore DJK, Mohamed MR, Sudhakar K, Peddakapu K. A new meta-heuristic optimization-based MPPT control technique for green energy harvesting from photovoltaic systems under different atmospheric conditions. Environ Sci Pollut Res 2023:1–16.
[26] Moghassemi A, Ebrahimi S, Padmanaban S, Mitolo M, Holm-Nielsen JB. Two fast metaheuristic-based MPPT techniques for partially shaded photovoltaic system. Int J Electr Power Energy Syst 2022;137:107567.
[27] Hassan A, Bass O, Masoum MA. An improved genetic algorithm based fractional open circuit voltage MPPT for solar PV systems. Energy Rep 2023;9:1535–48.
[28] Titri S, Larbes C, Toumi KY, Benatchba K. A new MPPT controller based on the Ant colony optimization algorithm for Photovoltaic systems under partial shading conditions. Appl Soft Comput 2017;58:465–79. https://doi.org/10.1016/j.asoc.2017.05.017.
[29] Bingöl O, Özkaya B. Analysis and comparison of different PV array configurations under partial shading conditions. Sol Energy 2018;160:336–43.
[30] Azizi M, Aickelin U, Khorshidi HA, Baghalzadeh Shishehgarkhaneh M. Energy valley optimizer: a novel metaheuristic algorithm for global and engineering optimization. Sci Rep 2023;13(1):226.
[31] Kennedy J, Eberhart R. Particle swarm optimization. In: *Proceedings of ICNN'95-international conference on neural networks*. IEEE; 1995. p. 1942–8.
[32] Yang X-S, Deb S. Engineering optimisation by cuckoo search. Int J Math Modelling Numer Optimisation 2010;1(4):330–43.
[33] Vicente EM, dos Santos Vicente P, Moreno RL, Ribeiro ER. High-efficiency MPPT method based on irradiance and temperature measurements. IET Renew Power Gener 2020;14(6):986–95.
[34] Ibrahim H, Anani N. Variations of PV module parameters with irradiance and temperature. Energy Procedia 2017;134:276–85.
[35] Gong Y, Wang Z, Lai Z, Jiang M. TVACPSO-assisted analysis of the effects of temperature and irradiance on the PV module performances. Energy 2021;227:120390.
[36] Mäki A, Valkealahti S. Effect of photovoltaic generator components on the number of MPPs under partial shading conditions. IEEE Trans Energy Convers 2013;28(4):1008–17.
[37] Mamun MAA, Hasanuzzaman M, Selvaraj J. Experimental investigation of the effect of partial shading on photovoltaic performance. IET Renew Power Gener 2017;11(7):912–21.
[38] Parlak KŞ. PV array reconfiguration method under partial shading conditions. Int J Electr Power Energy Syst 2014;63:713–21.
[39] Zafar MH, et al. Group teaching optimization algorithm based MPPT control of PV systems under partial shading and complex partial shading. Electronics 2020;9(11):1962.
[40] Mansoor M, Mirza AF, Ling Q, Javed MY. Novel Grass Hopper optimization based MPPT of PV systems for complex partial shading conditions. Sol Energy 2020;198:499–518.
[41] Bristow N, Kettle J. Outdoor performance of organic photovoltaics: Diurnal analysis, dependence on temperature, irradiance, and degradation. J Renew Sustain Energy 2015;7(1).